Available online at www.sciencedirect.com
SCIENCE DIRECT
Journal of Power Sources 158 (2006) 303–315
JOURNAL OF POWER SOURCES
www.elsevier.com/locate/jpowsour

Control strategy for a solid oxide fuel cell and gas turbine hybrid system

Christoph Stiller [a,*], Bjørn Thorud [a], Olav Bolland [a], Rambabu Kandepu [b], Lars Imsland [b]

[a] *Department of Energy and Process Engineering, Norwegian University of Science and Technology, Kolbjorn Hejes vei 1B, NO-7491 Trondheim, Norway*
[b] *Department of Engineering Cybernetics, Norwegian University of Science and Technology, NO-7491 Trondheim, Norway*

Received 8 April 2005; received in revised form 27 August 2005; accepted 6 September 2005
Available online 19 October 2005

Abstract

This paper presents a multi-loop control strategy for a SOFC/GT hybrid system. A detailed dynamic model of the system is presented and its part-load performance is studied. The control objectives are discussed, with the main issue being a fairly constant fuel cell temperature under all conditions. Based on the system configuration and part-load performance, input and output variables of the control system are detected. Control cycles are introduced and their design is discussed. The responses of the resulting system on load changes, external disturbances as well as malfunction and degradation incidents are investigated. The system is stable under all incidents. An error in fuel flow measurement or assumed fuel quality provokes a steady-state fuel cell temperature offset. For a degraded system, it may be advisable to readjust the control system to the new characteristics.

Keywords: SOFC; Hybrid cycle; Modelling; Part-load; Control

1. Introduction

A large amount of modelling work [1–4] and a demonstration plant [5] have proven that a solid oxide fuel cell (SOFC) integrated with a gas turbine (GT) has a potential for high efficiency electricity production with low environmental emissions. The good scalability of such systems makes them especially advantageous for distributed generation. Provided that quick load-following is feasible, stand alone power generation is a possible application.

However, SOFC/GT hybrid systems face many challenges when it comes to load change and part-load operation. A gas turbine alone has good dynamic properties, but part-load performance can be rather poor. At any operation point, compressor surge must be prevented. A SOFC is generally able to respond quickly to load changes [6], but it might be destroyed or seriously degraded either due to thermally induced stresses caused by different thermal expansion coefficients in the cell materials or from carbon deposition at the anode. Another phenomenon that may occur during load change is backflow of gas from the burner to the anode cycle, exposing the anode to oxygen. These incidents must not occur in any operation instance. Furthermore, for high efficiency and low degradation of the fuel cell due to thermal cycling, the fuel cell temperature should remain fairly constant during operation. The fulfilment of the mentioned tasks requires a comprehensive control strategy.

Results from part-load operation modelling have already been discussed by some authors. Costamagna et al. [7] investigated a hybrid system using a non-dimensional tubular SOFC model. In all simulations they assumed constant fuel utilisation (FU). If shaft speed was assumed constant, power output could only be controlled by varying the fuel flow. These simulations showed large variations in air utilisation (AU) and loss of efficiency for fixed shaft speed when operating at part-load. For variable shaft speed, however, AU and FU as well as SOFC inlet temperatures could remain fairly constant in part-load operation with only a small penalty on system efficiency. This effect was mainly due to increased recuperator efficiency owing to reduced air flow rate.

Campanari [8] also used a non-dimensional tubular SOFC model to investigate the hybrid system. Assuming constant FU of 80%, for constant shaft speed he suggested reducing AU and

Abbreviations: SOFC, solid oxide fuel cell; GT, gas turbine; FU, fuel utilisation; AU, air utilisation; TIT, turbine inlet temperature; TOT, turbine outlet temperature; IIR, indirect internal reforming

* Corresponding author. Tel.: +47 735 93723; fax: +47 735 98390.
E-mail addresses: christoph.stiller@ntnu.no (C. Stiller), bjorn.thorud@ntnu.no (B. Thorud), olav.bolland@ntnu.no (O. Bolland), rambabu.kandepu@ntnu.no (R. Kandepu), lars.imsland@ntnu.no (L. Imsland).

0378-7753/$ – see front matter © 2005 Elsevier B.V. All rights reserved.
doi:10.1016/j.jpowsour.2005.09.010

Nomenclature

Symbols

AF	air flow (relative to design value)
c	concentration (mol m^{-3})
c_p	heat capacity at constant pressure (J kg^{-1})
c_s	heat capacity of cell solid (J kg^{-1})
FF	fuel flow (relative to design value)
GP	generator power (relative to design value)
h	heat transfer coefficient (W m^{-2} K^{-1})
I	moment of inertia (kg m^2)
k	thermal conductivity (W m^{-1} K^{-1})
$\dot{m}$	reduced mass flow
n	reduced shaft speed
P	power (relative to design value)
P_b	shaft power balance (W)
r_{ij}	turnover of species i in reaction j (mol m^{-3} s^{-1})
r_s	radius of cell solid wall (m)
SM	surge margin
t	time (s)
T	temperature (K)
TF	temperature of fuel leaving the cell (relative to design value)
v	gas velocity (m s^{-1})
z	axial direction (m)

Greek letters

η_m	mechanical efficiency
π	pressure ratio
ρ	density (kg m^{-3})
ω	angular shaft speed (rad s^{-1})

Indexes

∞	ambient
comp	compressor
g	gas
gen	generator
i	species
s	cell solid
setp	setpoint
surge	surge condition
turb	turbine

current density for part-load. This approach will reduce power output of the SOFC as well as the turbine inlet temperature (TIT) and consequently the power output of the GT. For variable shaft speed he suggested to reduce air flow rate and current density to maintain a constant AU. However, a reduction in air flow rate leads to pressure reduction and therewith higher turbine outlet temperature (TOT) and thus higher recuperator outlet temperatures. Campanari concluded that for maintaining constant TIT, the current density has to be reduced further.

Chan et al. [3] also investigated a non-dimensional tubular SOFC-type in a hybrid system. In their system, power is reduced by shifting the load from the SOFC to the GT through introducing fuel to the combustor, which results in strong reduction of the system efficiency. This method also implies that a SOFC bypass should be implemented for both fuel and air. Due to the low part-load efficiency, they state that this method is mainly for short term load reduction. The aim was to maintain a relatively high SOFC temperature.

Pålsson and Selimovic [9] used a two-dimensional planar SOFC model for part-load studies. Design point was set where the compressor flow matched the cooling requirement of the SOFC. They introduced an air heater/cooler prior to the SOFC entry in order to meet the requirements for the air inlet temperatures at part-load operation. TIT was kept constant and shaft speed was varied. At part-load operation, increased FU and low GT part-load efficiency led to increased power contribution from the SOFC. Due to the problems associated with matching of the system components, they concluded that the load range for hybrid systems should be limited to 55–100%, corresponding to a load variation of the GT of 20–100%.

Kimijima and Kasagi [10] studied part-load of a 30 kW simple recuperated cycle using a non-dimensional SOFC model and compared variable and fixed shaft speed operation. FU was kept constant, even though it is mentioned that FU could be increased at part-load operation. They conclude that variable shaft speed operation is favourable in terms of part-load performance; however the higher TOT could cause problems.

Some of the authors of the present work have recently presented a complex model of a SOFC/GT system [11]. Performance maps were introduced to illustrate the variations of the most important parameters over the two degrees of freedom, namely shaft speed and fuel flow. Based on these maps, it was found that strategies with fairly constant temperatures in the SOFC seem feasible but require a feedback control system for safe operation. Responses of the non-controlled system on variations of shaft speed and fuel flow were briefly studied.

All above-mentioned authors have identified inlet and outlet gas temperatures as well as air and fuel utilisations of the SOFC as important parameters for part-load operation of hybrid systems. Maintaining a constant SOFC operation temperature is important to avoid thermal cracking, but this might be difficult to achieve at reduced pressure as the TOT and consequently the recuperator outlet temperature increases.

A few studies on control layout and load-following of high temperature fuel cell systems and hybrid systems have been published so far. Zhu and Tomsovic [12] have studied the load-following of microturbine and fuel cell system models, however not as a hybrid system but as separate systems coupled together in a power network. Response time of approximately 10 and 30 s were observed for load increase in the microturbine and SOFC system, respectively. The slow SOFC response was mainly due to the slow dynamics of the fuel processor. It was concluded that load-following in a network is to be provided mainly by microturbine systems. Jurado [13] designed a control system for a molten carbonate fuel cell indirectly integrated into a gas turbine. Controllers for the gas turbine and fuel cell are introduced; however no coupling between these is established. Both references do not regard the thermo- and gas-dynamical processes during and subsequent to load changes.

The aim of the current work is to present a comprehensive control layout for a hybrid system. A detailed dynamic model of a tubular SOFC system integrated into a simple recuperated GT cycle as the basis for the investigation is described. The steady-state behaviour of the system is displayed in performance maps. Next, control objectives and the nature of disturbances influencing the system are discussed. A combined feedback–feedforward control layout is introduced. From the performance maps, an appropriate operation line is selected and the feedforward section is tuned to it. Feedback controller tuning is discussed. As a result, the responses of the controlled system to certain load changes and disturbances are studied.

2. Hybrid cycle model

The investigated hybrid cycle is shown in Fig. 1. The SOFC system design (inside the vessel in Fig. 1) is similar to that of Siemens–Westinghouse [14,15]. The model incorporates indirect internal reformer (IIR), afterburner and recirculation and mixing chamber, where part of the anode exhaust gas is admixed to the fresh fuel in an ejector in order to supply steam to the steam reforming and shift reaction. Required valves for start-up, shutdown and failure have not been included.

Since the last study [11] with this hybrid cycle model, the reforming section has been improved. Furthermore, heat loss from the stack by radiation has been added and the activation and diffusion potential models have been refined. The models are described below.

2.1. SOFC

The SOFC model is spatially discretised and fully dynamic in terms of gas transport and heat transfer, allowing the study of temperature distributions. Gas flows are treated as 1D plug flows:

$$\frac{\partial c_i}{\partial t} + v_g \frac{\partial c_i}{\partial z} = \sum_j r_{i,j} \tag{1}$$

The solid structures are modelled by a 2D discretisation scheme in axial and radial direction, neglecting effects in the circumferential direction. Heat conduction in solid structures is calculated by

$$\frac{dT_s}{dt} = \frac{k_s}{c_s \rho_s} \nabla^2 T_s \tag{2}$$

Internal reforming is implemented using the kinetic approach of Achenbach [16] for steam-methane reforming, while the water-gas shift reaction is assumed to be always in equilibrium. The model calculates the local electrical potential balance, accounting for the effects of activation (Butler–Volmer) and diffusion

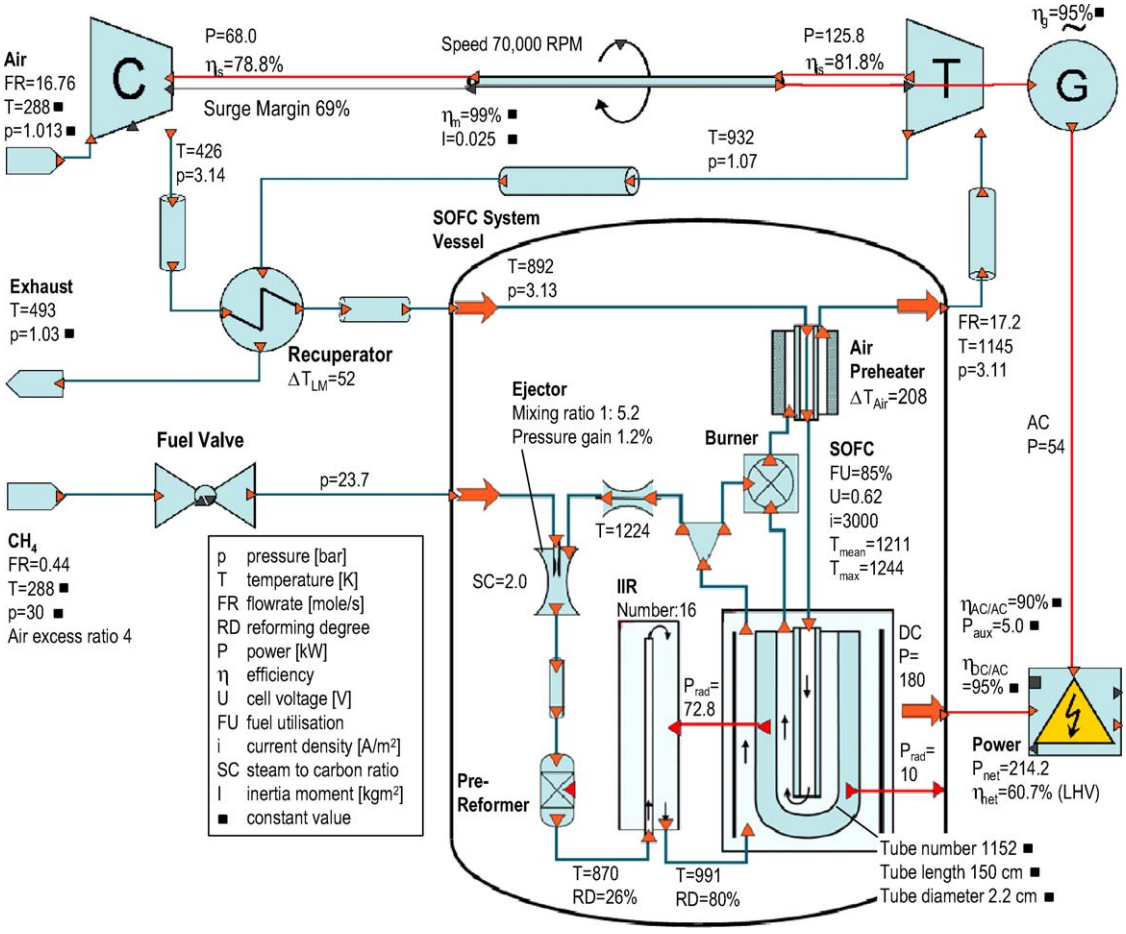

Fig. 1. Hybrid cycle layout and design point values (square marked values remain always constant).

potentials (Fick's law and Knudsen diffusion) and ohmic resistance. The constants used in the Butler–Volmer equation have been estimated based on measurement data from Singhal and Kendall [17]. For the heat transfer between the solids and the gases, Newton's law of cooling is applied in the following way:

$$\frac{\partial(T_g c_{p;g}\rho_g)}{\partial t} + v_g \frac{\partial(T_g c_{p;g}\rho_g)}{\partial z} = \frac{2h}{r_s}(T_s - T_g) \quad (3)$$

Spatially discretised radiation heat exchange is included between the cathode surface and the air supply tube. Furthermore, the anode radiates to the IIR to supply heat for the reforming reaction, and to the casing wall, leading to heat loss to the environment. Friction losses in the gas channels are accounted for by the Reynolds number approach.

2.2. Anode recirculation loop and reformers

In order to supply steam for the reforming process, a certain part of the anode exhaust gas must be recycled. The suction of the recycle stream and the mixing with the fresh fuel is performed by an ejector. High induced (recycle) flow rates at low pressure differences are typically achieved by subsonic mixing ejectors. The actuating flow is accelerated to supersonic speed in a Laval nozzle before it enters the mixing chamber. The ejector model is based on section-wise momentum balances and has been validated against data from Marsano et al. [18]. Pressure losses are included by a fixed throttle valve. Ejector behaviour is difficult to model without experimental validation and hence a practical ejector might differ from the model.

Before entering the anode, the gas leaving the ejector passes through two reformers: an adiabatic pre-reformer and an internal indirect reformer (IIR). The pre-reformer is modelled as a non-dimensional Gibbs equilibrium reactor where reforming and water-gas shift reactions take place. It is meant for cracking any higher hydrocarbons in the fuel gas and reform a part of the methane until equilibrium is reached. To account for reaction kinetics, a difference between the actual outlet temperature and the equilibrium temperature of 20 K is assumed.

The IIR is situated downstream the pre-reformer and it is based on Gibbs equilibrium. The gas is assumed to be reformed while flowing downwards rectangular ducts. The duct walls are coupled to the fuel cell anode by radiation. The latter is discretised in flow direction. A view factor is adjusted in the design calculation to meet the desired reforming degree. Gas residence time in the reformer is accounted analogously to the SOFC model (Eq. (1)). For accurately modelling reformer behaviour, its geometry and reaction kinetics must be regarded. For the present study, the modelling approach including thermal inertia of the reformer wall is however rated as sufficient.

2.3. Burner and recuperators

The burner is modelled non-dimensionally and adiabatically and completely combusts the remaining anode exhaust gas together with the cathode air. The mixing cathode and anode exhaust streams causes pressure equalisation of these flows upstream. In practice, difficulties may appear with reliably combusting highly depleted fuel.

The burner exhaust preheats the inlet air by a counter-flow tube-shell set-up, where the tube is the prolongation of the fuel cell air supply tube. The model accounts for thermal inertia, pressure loss and gas residence times, using the same approaches as in the SOFC model.

The recuperator heat exchanger is a stack of counter-flow plate-fin type. A two-dimensional distributed model is applied that accounts for thermal inertia, pressure loss and gas residence times. The recuperator model is based on data and relations from Kays and London [19].

2.4. Gas turbine

The gas turbine features map-based steady-state turbomachinery models, a shaft model accounting for rotating mass inertia, power electronics and ducts.

The compressor is based on the performance map of a small centrifugal research compressor by the German Aerospace Centre, found in a map collection from Kurzke [20]. The map is understood as a generic radial compressor map. Therefore it has been scaled in terms of reduced mass flow, pressure ratio and shaft speed to fit the design case. The map has been modelled using polynomials of fourth and fifth order for reduced mass flow, pressure and efficiency as functions of reduced shaft speed and operation (β) line. A surge margin (SM) is calculated as follows:

$$\mathrm{SM} = \frac{\pi_{\mathrm{surge}}(\dot{m}) - \pi(\dot{m}, n)}{\pi(\dot{m}, n)} \quad (4)$$

where $\pi(\dot{m}, n)$ is the actual pressure ratio at the actual reduced mass flow and reduced shaft speed and $\pi_{\mathrm{surge}}(\dot{m})$ the surge pressure ratio at the actual reduced mass flow.

The turbine is based on the performance map of a small radial turbine [20] which also is scaled to fit the design case. An ellipse approach has been used for the relationship between reduced mass flow, reduced shaft speed and operation (β) line. Pressure ratio and efficiency have been modelled by a polynomials approach.

Generator and power electronics account for transformation efficiencies which are assumed to be constant. A constant power sink accounts for power consumption of auxiliaries and transformation efficiency decrease at low load.

The shaft model includes acceleration/deceleration of the shaft through moment of inertia of the moving parts:

$$\frac{\mathrm{d}\omega}{\mathrm{d}t} = \frac{P_b}{I\omega} \quad (5)$$

where ω is the angular shaft speed in rad s^{-1}, I the moment of inertia in kg m^2, and P_b the power balance:

$$P_b = \eta_m P_{\mathrm{turb}} - P_{\mathrm{comp}} - P_{\mathrm{gen}} \text{ in W} \quad (6)$$

The ducts have the purpose to account for gas residence time in the piping. Heat and pressure losses and thermal inertia of the ducts and gas turbine components are neglected, as

they are considered to be minor compared to the SOFC system. This might lead to a slight overestimation of the system efficiency.

2.5. Complete model

The complete model is implemented in gPROMS [21], a process modelling tool based on an equation oriented solver. The strength of the equation oriented approach is that there is no fixed input–output structure. In fact, a certain number and combination of variables must be specified in order to achieve a valid equation system, but many degrees of freedom remain in choice of variables. As an example, either voltage or current of the fuel cell model may be specified.

The resulting system model consists of approximately 14,000 algebraic and 2300 state variables. The simulations were performed on a 2.5 GHz Intel Pentium-4 processor PC. Calculation time for a steady-state point was approximately 5–10 s. The solver used for dynamic calculations (SRADAU) varies time increments, thus calculation time depends on the occurrence of discontinuities and momentary fluctuation rate of the variables. A calculation time of about 5 min was required for the load change studies shown below, while the load profile simulation required about 20 h.

3. Design case and steady-state part-load behaviour

Before part-load behaviour can be studied, a design point must be defined. All relevant cycle data are displayed in Fig. 1. Most of the data are similar to recent literature on hybrid cycles [3,7,8,10] and public data from Siemens–Westinghouse. Values in the figure marked with a square are constant during all simulations. The design point and system dimensioning is furthermore based on the following assumptions:

- The system size is determined on the basis of the Siemens–Westinghouse stack design which incorporates 1152 tubular cells [22] and 16 indirect internal reformers.
- Pure methane is supplied as fuel.
- The view factor for the radiation from the anode surface to the IIR is equal for each cell and has been adjusted to achieve a reforming degree of 80%. High external reforming degrees cause flatter profiles of temperature and current density in the cell. Song et al. [15] report that the IIR exhaust gas includes only a small amount of unreformed methane at the Siemens–Westinghouse configuration.
- The view factor for the radiation from the anode surface to the stack casing has been adjusted in order to obtain a guessed heat loss at design point. A value of 10 kW is regarded as realistic and feasible.
- A length of 0.5 m was chosen for the air preheat tube, yielding a temperature increase of 208 K at design point. The length of the air preheat tube significantly influences the SOFC temperature.
- The ducts have a length of 1 m and are dimensioned for gas velocities of approximately 20 m s^{-1} at design point. The residence times are calculated utilising the ideal gas law. Residence times before and after the pre-reformer account for the actual pre-reformer residence time.
- The fuel utilisation (FU) is determined from current and fuel flow, as these parameters can be measured in a real system. Setting FU constant hence means maintaining a constant ratio of current to fuel flow. While this in steady-state provokes a constant content of combustibles in the anode exhaust gas, the content may vary during dynamic operation due to pressure change and gas transport delay. Due to the variations in heating value of the exhaust gas, severe oscillations in burner temperature may occur during load change. The common fuel utilisation value of 85% has been chosen.
- The ejector has been dimensioned for supplying a steam to carbon ratio of 2 in the design point. The difference in static pressure of induced and actuating gas flow in the mixing zone is vital for the ejector performance. According to Johannesen [23], a lower actuating flow pressure than induced flow pressure causes a strong reduction in induced flow rate. In contrast, a higher actuating flow pressure does not significantly increase induced fluid flow rate. For being able to reduce the fuel flow rate for part-load operation while maintaining a high recycle ratio, the inlet pressure of the actuating fluid at design point must be high. A value of 23.7 bar was chosen for design point. It is assumed that natural gas is available at high pressure, and hence there is no need for a fuel compressor.
- The recuperator is dimensioned in order to achieve a high amount of heat recuperation at tolerable size and pressure drop.
- The total moment of inertia for the rotating parts (turbine, compressor, generator and shaft) is assumed to be 0.025 kg m^2. This is equivalent to a rotating mass of 20 kg and a mean radius of 5 cm. The moment of inertia influences the power output during shaft acceleration and deceleration.
- The generator is assumed to have a constant efficiency of 95%. The power electronics have constant efficiencies of 90% for AC/AC and 95% for DC/AC conversion. As a comparison, von Spakovsky et al. [24] report values of 92–95% for DC/AC conversion for a 5 kW system. In order to account for power consumption of auxiliaries and the decreasing conversion efficiencies at load reduction, a constant power loss of 5 kW was applied.

With the given design and assuming a constant fuel utilisation in steady-state operation, two degrees of freedom remain for off-design operation, most pragmatically expressed by the parameters of fuel and air flow rate. Fuel flow can be controlled by a flow control valve. The air flow can be controlled through the gas turbine system in various ways; such as variable shaft speed, variable compressor inlet guide vanes or variable compressor bleed. Their effect on the system is very similar. Shaft speed variation is the option maintaining the highest efficiencies and the lowest pressure changes when reducing air flow. It was therefore selected here. The shaft speed is controllable through the power that is produced by the generator.

The free parameters air and fuel flow may be varied independently from each other within certain limits. Each

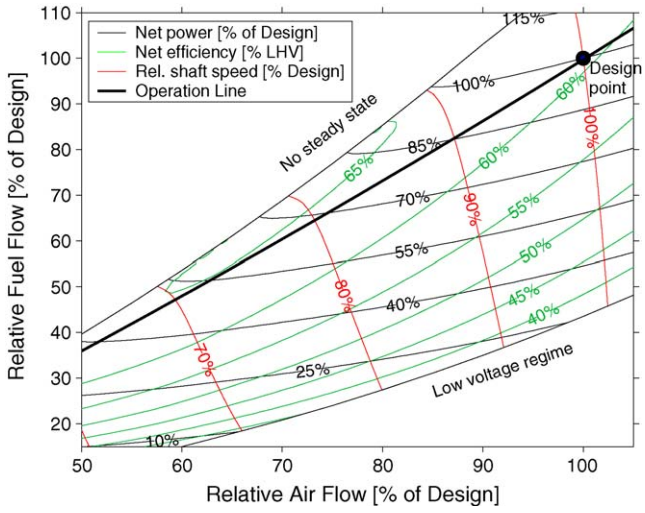

Fig. 2. Steady-state performance: power, efficiency and shaft speed.

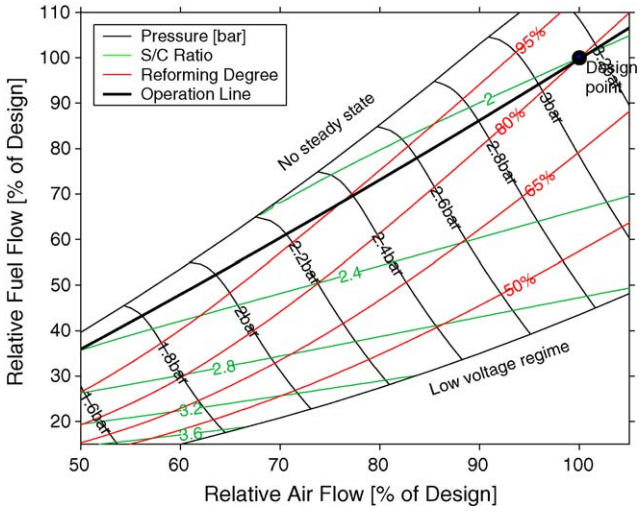

Fig. 4. Steady-state performance: pressure, steam-to-carbon ratio and reforming degree.

combination determines a certain operation point of the system. Figs. 2–4 show the steady-state behaviour of the parameters of interest as a function of fuel flow (FF) and air flow (AF) relative to their design values. Similar maps have been introduced for an SOFC stack system [25] and a full hybrid system [11].

In the blinded out regime on the upper left (low air and high fuel flow), no steady-state operation exists. Transient simulations have shown that the temperature in this regime is steadily climbing far beyond the valid ranges and eventually causing compressor surge. This is because enhanced effectiveness of the heat recuperation loop and lower air excess ratio at lower airflow causes TIT to increase.

In the lower right regime (high air and low fuel flow), the fuel cell is cooled down strongly and therefore the voltage is low. As it is not recommendable to operate in this regime, it is blinded out for cell voltages lower than 0.3 V.

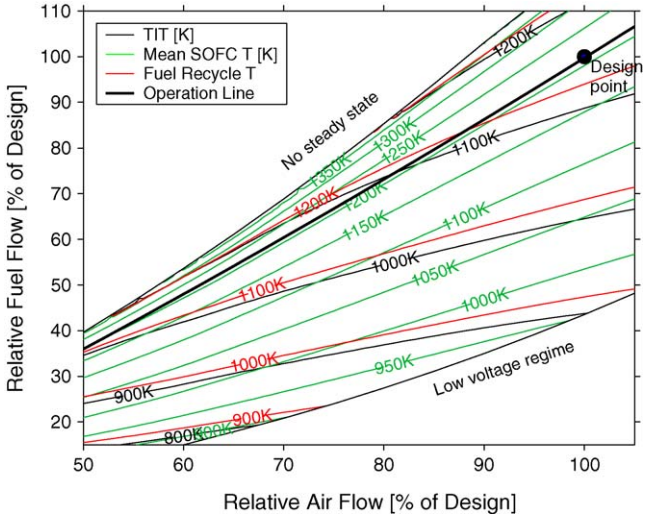

Fig. 3. Steady-state performance: TIT, mean SOFC and fuel recycle temperature.

A first result from the performance map is that reducing fuel flow at constant air flow, i.e. going down a vertical line from the design point, results in a strong reduction in temperatures and therewith efficiencies.

The figures also show that a load reduction by linearly reducing fuel flow and air flow will lead into the unstable region. Remaining in the stable regime therefore implies larger relative reduction in fuel flow than air flow. This is a consequence of the lower pressure ratio at lower shaft speed which results in an increased TOT. The same behaviour is also confirmed in a study by Costamagna et al. [7].

Surge margin and steam to carbon ratio do not reach any alarming values in the shown operation range.

4. Control design

4.1. Control objectives

A suitable control strategy for normal operation must meet the following objectives:

- *Safe operation of the system*: Incidents which may cause damage to the fuel cell or other components must be avoided. Such incidents are compressor surge or cell degradation due to thermal cracking or too high temperatures, carbon deposition and therewith blocking of the anode, and backflow of gas from the burner to the anode cycle, exposing the anode to oxygen. Compressor surge can occur in case of too high turbine inlet temperature. The occurrence of thermal cracking is coupled to the temperature and therewith stress profile in the cell. A model for thermal stress calculation in tubular SOFC has been developed recently at NTNU [26], however it is very computationally expensive and revealed a high degree of uncertainty and sensitivity to exact material properties. Carbon deposition occurs with too low temperatures and too low amount of steam at the cell inlet. Anode backflow has been observed with the

model used here during sharp pressure increases [11]. It is therewith restricting the maximum allowed pressure increase rate.

- *Quick load-following and high efficiency*: The selected control strategy should make it possible to follow a load profile quickly and accurately and furthermore maintain a high efficiency of the system in part-load operation.
- *Long lifetime of the fuel cell*: In addition to thermal cracking, the fuel cell may be degraded due to thermal fatigue and high local heat production rates [24]. The effect of thermal fatigue may be reduced by reducing the thermal cycling amplitude. Hence the mean cell temperature should be maintained as constant as possible throughout any part-load operation. Local heat production may be controlled by limiting the current drawn from the cell.
- *Governing external influences*: The system must react on external disturbances and adapt to changes in subcomponent performance, caused for example by fuel cell degradation or compressor fouling.

4.2. Analysis of the system

The hybrid cycle model is strongly non-linear and cannot be easily linearised due to its complexity. Therefore, most of the common controllability analysis techniques are not applicable [27]. However, having mapped the part-load behaviour, the system response is not so difficult to predict and thus the system is analysed manually.

The system has only one outer control variable, which is power. However, a certain operation strategy must be implemented, and thus also fuel utilisation, air flow and SOFC temperature have to be controlled. The manipulated variables are current, fuel flow and generator power.

There is strong interaction among the manipulated and controlled variables. However, as the required time scales are very different for the different control issues, a multi-loop control design may be applied without resulting in instabilities:

- Power is controlled by manipulating SOFC current due to its quick dynamics (magnitude of less than one second).
- Fuel utilisation must hence be controlled by manipulating the fuel flow (magnitude of few seconds).
- Air flow is controlled by manipulating the generator power and thus adjusting the shaft speed (magnitude of 1 min).
- Cell temperature is controlled by adjustment of the air flow setpoint (very slow).

The mentioned control loops are explained in detail in the following sections. The resulting control system is sketched in Fig. 5.

It must be pointed out that the control strategy presented here is adapted to the behaviour of the described system. Even though the shown parameters are only valid for this system, it is expected that the control strategy can be adapted to a real system once data of its true behaviour are available.

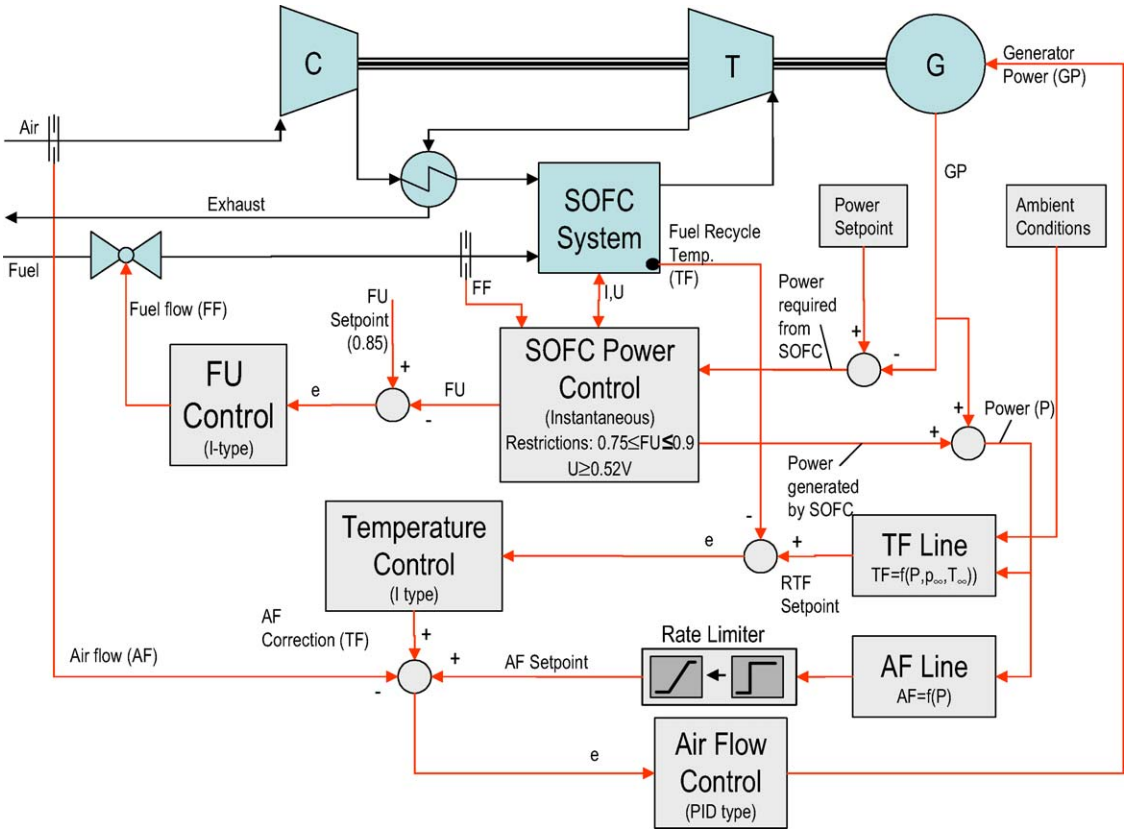

Fig. 5. Control system design.

4.3. SOFC power controller

The fuel cell can respond very quickly to load changes, as it is only limited by the electrochemical reaction restoring the charge which has been drained by the load [12]. Typically, time constants of below 1 s are assumed for a change in current [12,24]. For the primary control of power, it is therefore reasonable to manipulate the fuel cell current. It is assumed that this is done instantaneously by the power electronics subsystem which determines the operation point on the current–voltage line of the fuel cell. However, there are some limitations that prohibit the arbitrary movement on this line:

- The fuel utilisation must be kept within certain bounds. A too low FU leads to low steam content in the anode recycle and high TIT and therewith the risk of carbon deposition and compressor surge. A too high FU on the other hand leads to steep internal temperature gradients in the fuel cell and therewith advances thermal cracking. It is chosen to vary fuel utilisation in the range from 75 to 90%.
- The cell voltage must not drop under a certain level, as there is a maximum power output at an intermediate voltage (approximately 0.5–0.6 V, depending on the operation state). Lower voltage causes decreasing power in spite of increasing current and is unfavourable. A minimum voltage of 0.52 V is chosen.

The outcome is a multi-mode controller which switches between the modes of "*normal operation*", "*maximum FU*", "*minimum FU*" and "*minimum voltage*" to fulfil all above limitations. In "*normal operation*" mode, the current is manipulated so that the desired power of the whole system is produced. Small load steps in the range of some kilowatts can be followed instantaneously, while for larger steps, the controller switches to the mode "*maximum FU*" or "*minimum voltage*" in case a load increase and "*minimum FU*" in case of a decrease.

4.4. Fuel utilisation control

After a load change, the fuel utilisation must be reset to its static value of 85%. This is achieved simply by an indirect acting integral controller (integral time constant of 10 s), to which the fuel utilisation error serves as input and which manipulates the setpoint of the fuel flow valve. If the SOFC power controller is in "*normal operation*" mode, it will remain in this mode and the fuel utilisation will be reset to its static value. If it is in "*maximum FU*" mode, i.e. during a larger load increase, at first the error remains constant and the fuel utilisation controller will increase the fuel flow in a linear ramp function. At the point where the SOFC power controller can satisfy the power demand, it switches back to "*normal operation*", and the fuel flow ramp flattens to finally reach the new steady value. Zhu and Tomsovic [12] have previously shown a control strategy where fuel utilisation is reaching a high boundary during load increase.

4.5. Air flow control

The above-mentioned controllers fix the fuel flow. From the performance maps (Figs. 2–4) it can be seen that a fuel flow change should not be undertaken without a corresponding change in air flow, or the system will advance to unfavourable conditions. In Fig. 3 it can also be seen that a constant mean solid temperature is achievable over a load range from 40 to approximately 105%. Moreover, this operation line features a high efficiency in part-load. From the map data, a characteristic line for the air flow as a function of fuel flow or power can be developed which provides a setpoint to the air flow controller. However, the fuel flow will tend to overshoot the target values during load changes. This might cause instability in the system if fuel flow is taken as input to the air flow setpoint calculation. Hence, a controlled parameter is chosen, i.e. the produced power. The result is a characteristic function for the air flow setpoint (AF_{setp}) as a polynomial function of power (P) at constant mean solid temperature of the shape $AF_{setp} = f(P)$.

The setpoint together with the measured signal forms the error for the air flow feedback controller, which is an indirect acting proportional-integral-differential (PID) type. It manipulates the generator power (GP) through sending a power setpoint to the power electronics. We assume the power electronics to be able to instantaneously adjust the power drawn from the generator to this value.

With a given constant generator power, the system is at an unstable equilibrium. Departing from steady-state, for example, a step increase of the generator power will lead to deceleration of the shaft speed. No new equilibrium will be found within the valid bounds of shaft speed. By trial-and-error tuning, it has been found that a PID type controller with a high gain of ~8, an integral time constant of ~18 s and a differential time constant of ~0.8 s is able to control the shaft speed and air flow reliably, stably and quickly. However, a too quick change of the air flow rate is not desirable, as this may lead to anode backflow, inverse reaction of system power due to high amplitudes in generator power and instability due to interference with the fuel utilisation control. In order to slow down the air flow change rate, the air flow setpoint signal is smoothened by a rate limiter.

Air flow and shaft speed are directly coupled. Nevertheless, for example a change in air density may lead to a higher required shaft speed for maintaining a certain air flow rate. Therefore the shaft speed must be monitored and overspeed protection must be provided.

4.6. Temperature control

Under ideal conditions, the above-mentioned strategy is able to follow a load line while maintaining safe operation and constant temperature. However, the strategy does not yet assure a stable cell temperature upon external disturbances as well as changes in system characteristics through degradation, or measurement errors. Especially in the low load regime, the cell temperature is very sensitive to the fuel flow. A small error of 1–2% points (caused by valve measurement error or varying fuel quality) may lead to steady-state temperature change of 50 K, even though it must be noted that the temperature advances very slowly to its new steady value (in the magnitude of hours to days). As the control strategy must also ensure temperature stability, an additional feedback loop is required.

An effective way to control the temperature by only influencing the power slightly is by manipulating the air flow (see almost horizontal power iso-lines in Fig. 2). An obstacle is that the mean cell temperature cannot be measured conveniently. However the related temperature of the fuel leaving the cell (TF) can be measured, for example in the recirculation plenum.

An implicit relationship between the two temperatures is established by once again determining a characteristic line. It has been detected that apart from the load, the relationship is dependent on the ambient air conditions. The setpoint of TF is hence calculated as a second order polynomial function of power, ambient pressure and ambient temperature; $TF_{setp} = f(P, p_\infty, T_\infty)$. The coefficients of this function have been fitted using the least squares method on simulation results with constant mean cell temperature.

The error from setpoint and measured fuel temperature is fed into a slow, direct acting integral controller (integral time constant of 20,000 s). A quicker controller would react too strongly on load change dynamics which provoke a temporary error in fuel temperature. The controller output signal is added to the air flow setpoint entering the air flow controller. This method of controlling a non-measurable variable indirectly by a measurable one is called inferential control [27].

5. System response results

5.1. Small load change

Small distributed networks supplying private households are assumed to have a maximum step change of power of about 10 kW (4.7% power). Figs. 6 and 7 show the system response to a load decrease, respectively, increase of this step size around design condition over a logarithmic time axis. At the power decrease, the setpoint power is reached after less than 1 s without the SOFC power controller reaching the "*minimum FU*" limit. At the load increase, the SOFC power controller switches to "*maximum FU*" for approximately 3 s before the setpoint power is reached. Air flow advances gently to the new point of the characteristics, while the fuel flow varies in order to keep the fuel utilisation at its setpoint value. The values are fairly steady after approximately 20 s. The cell temperature variation of approximately 2 K is due to the thermal inertia of the indirect internal reformer, which causes the reforming degree at the cell entrance to adapt slowly to the new steady-state. This affects the energy balance of the cell and therewith causes the temporary temperature variation. With greater time constants, the temperature resets to its design value.

5.2. Large load change

For industrial applications, larger load changes than the above may occur. In the following, the system response to a load change of 100 kW (from rated power down to 53%) is investigated and shown in Figs. 8 and 9. The setpoint power is reached after approximately 11 and 57 s at the load decrease and increase, respectively. The slower response at power increase is due to the lower deviation of fuel utilisation from its setpoint. It is furthermore technically required due to the risk of backflow from the burner into the anode recirculation system during pressure increase (this being not an issue at pressure decrease). A faster load increase may be achievable through higher gain of the fuel utilisation controller. Furthermore, the mean cell temperature reaches a minimum of 29 K below the design point approximately 1100 s after the load decrease and a maximum of 35 K above design point approximately 600 s after the load increase. This is again due to the IIR thermal inertia as mentioned above. The presented control strategy is hence able to stabilise the mean cell temperature in a bandwidth of 65 K under strong and quick load fluctuation.

5.3. Load profile

To demonstrate the stability of the cell temperature during load-following, the system is exposed to a randomly generated 24 h load profile. It implies average 24 random steps per hour

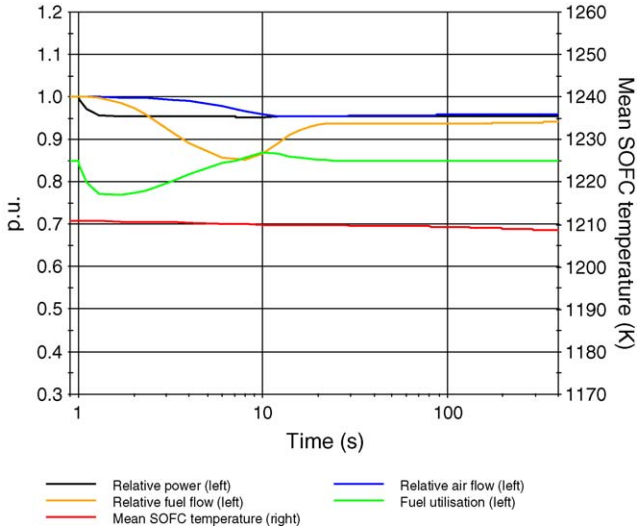

Fig. 6. Response to small load decrease (−4.7%).

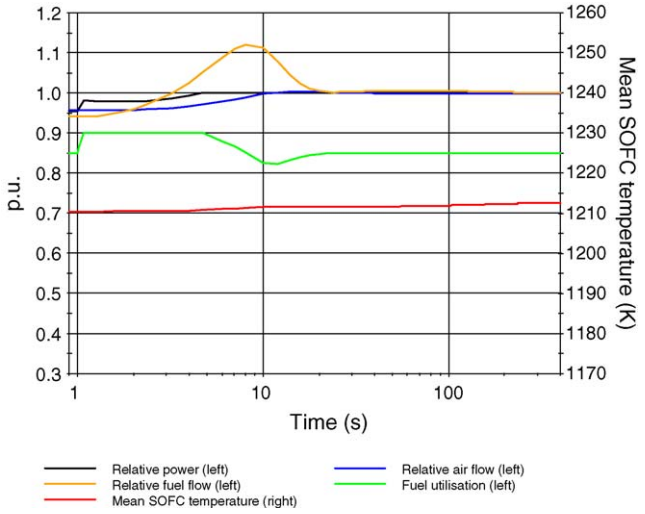

Fig. 7. Response to small load increase (+4.7%).

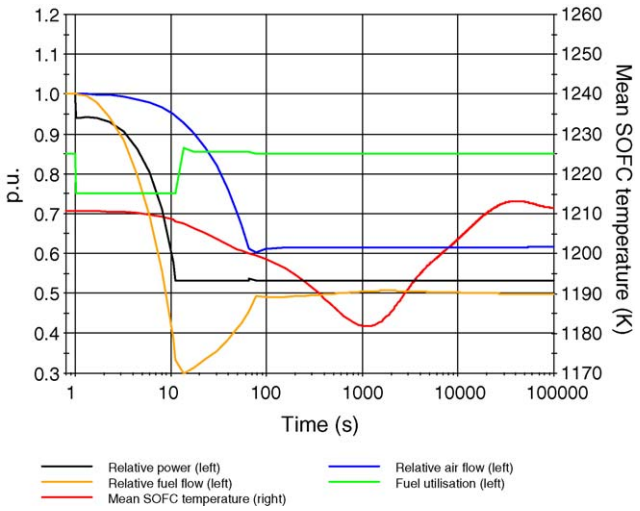

Fig. 8. Response to large load decrease (−47%).

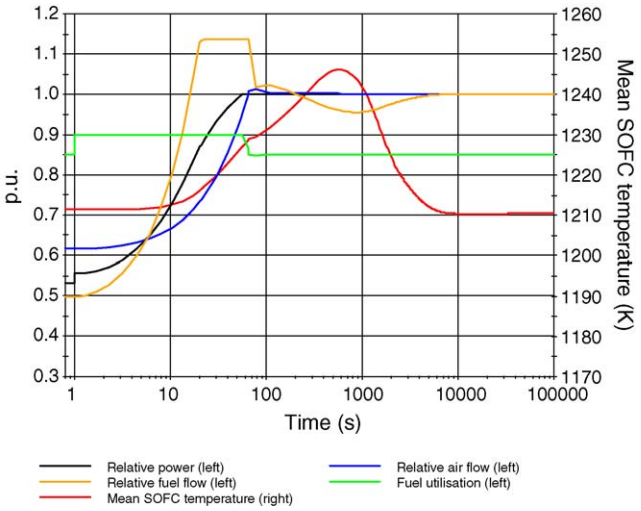

Fig. 9. Response to large load increase (+47%).

with a maximum size of 10 kW. Furthermore, a day–night variation covering the full load range of 40–105% is superposed. Fig. 10 shows the load line and the system parameters. Under these conditions, the observed bandwidth of the temperature is approximately 40 K. The strongest deviations result from steep load increase and decrease.

5.4. Ambient pressure and temperature change

In practice, the system is exposed to external disturbances, such as ambient pressure and temperature variation. These usually vary in the magnitude of hours. The response to a simultaneous temperature increase of 15 K and pressure decrease of 20 mbar over a time of 1 h, corresponding to a decrease of air density of 8%, has been studied.

In Fig. 11 it can be seen that after the change, the mean cell temperature increases about 7 K, as a higher air flow is required under these conditions. As the temperature control considers the measured ambient conditions, it is able to reset the cell temperature to the original value, however in a time scale of several days. It is therewith sufficient for compensating annual, but not daily fluctuations.

The effect of ambient air density could be compensated very quickly through a feedforward control which is providing an additional correction of the air flow setpoint. However, it has been shown that the cell temperature oscillations due to load cycling are higher than the ones caused by ambient conditions.

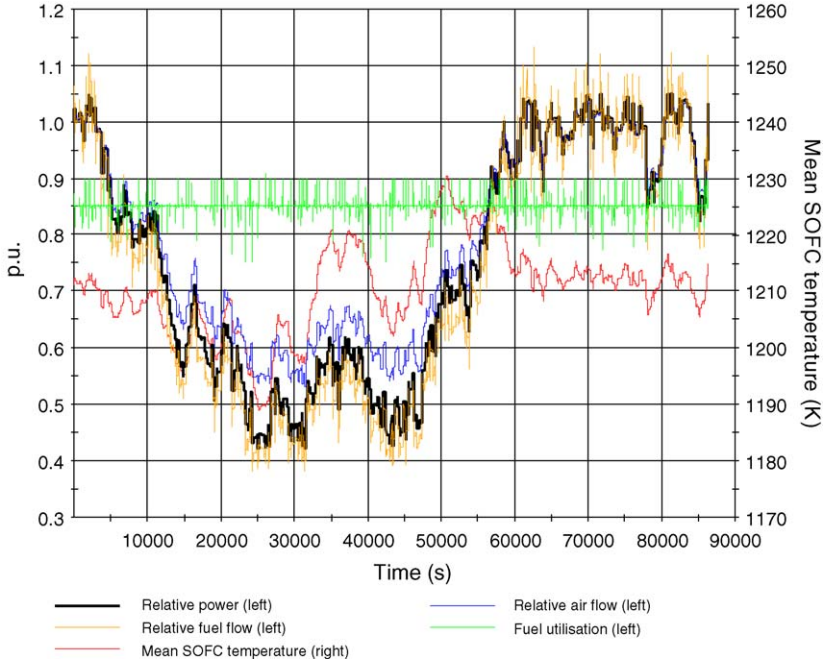

Fig. 10. Response to load profile.

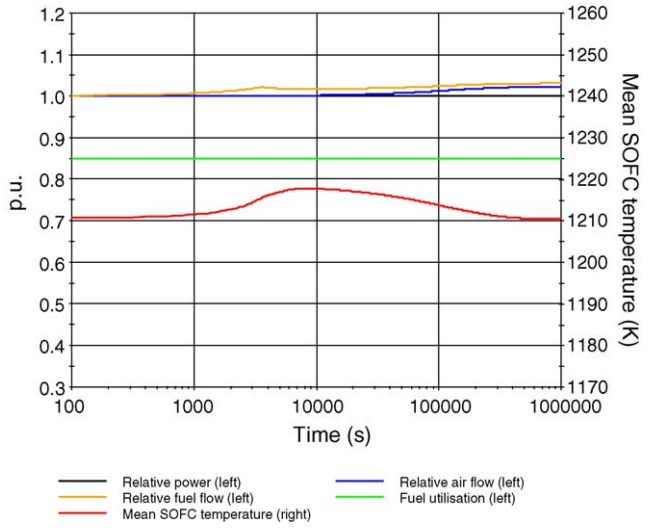

Fig. 11. Response to change in ambient conditions (+15 °C, −0.02 bar).

Hence, it is not considered as necessary under the given conditions.

5.5. Malfunction and degradation

The system characteristics shown in Figs. 2–4 are subject to changes during the system life due to degradation of the components. Furthermore, malfunction of the measuring may affect system stability. It is hence important to check the stability of the control system under these changed conditions.

In order to simulate fluctuation of load, we exposed the system to a sinusoidal oscillation between 53 and 100% of power with a period of 2000 s. Initially, the ordinarily working system is at steady-state. At time zero, the following incidents occur one at a time:

- *Fuel cell degradation*: An additional ohmic resistance is implied on the fuel cell, provoking a voltage loss of 50 mV at design current.
- *Compressor fouling and degradation*: Compressor design efficiency, flow rate and pressure ratio are decreased by 3%.
- *Fuel measurement malfunction*: Fuel flow is overestimated by 5%. This incident is similar to a change in the heating value of the fuel feed.
- *Air measurement malfunction*: Air flow is overestimated by 5%. Lower air flow leads to a higher mean SOFC temperature and is thus challenging the temperature control.

The resulting mean cell temperature responses are shown in Fig. 12. It can be seen that the temperature control system tackles all disturbances and the temperature always stays within an acceptable range. Nevertheless, steady-state deviations of the temperature occur in some cases. This is because the inferential control scheme is disturbed by a changed relationship between measured and controlled temperature. The effect is strongest for fuel measurement malfunction, as this leads to a falsified fuel utilisation, to which the system characteristics are very sensitive. Precise and possibly redundant measuring of the fuel flow and furthermore certainty of the fuel quality is thus recommended. The fuel cell degradation simulation shows a high peak of the temperature shortly after the incident. However, degradation effects usually occur gradually, and this peak will therewith not occur in practice. On the other hand, an increase in the temperature amplitude is also visible. This is due to mismatching of the real and assumed characteristics and may be eliminated by readjustment of the controller characteristics after a certain lifetime.

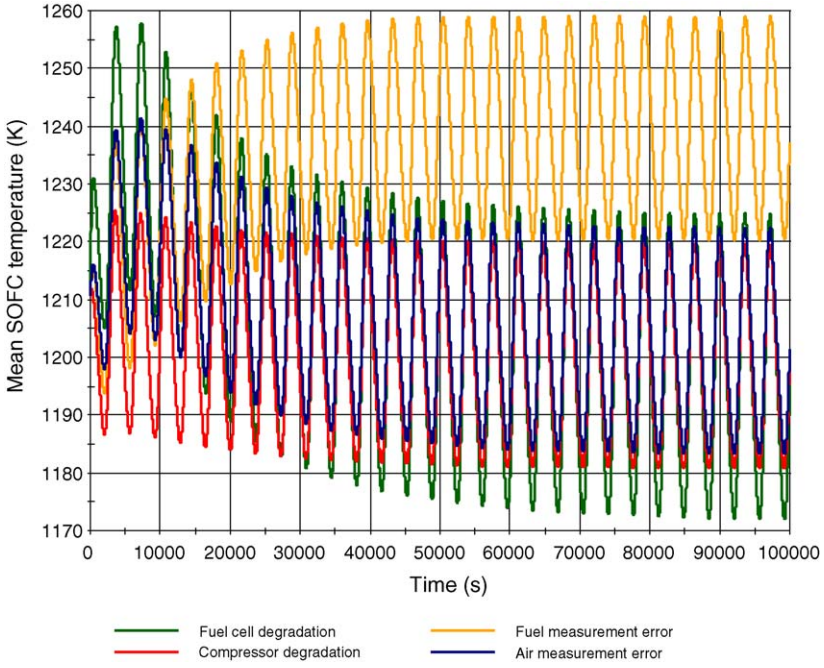

Fig. 12. Mean cell temperature response to malfunction and degradation effects.

Beside the mentioned malfunctions, several other and more severe malfunctions can occur, which the control system cannot tackle. A practical control system must therefore supervise further process parameters and if necessary run a safety shut-down routine to protect the hybrid system. This however exceeds the scope of this study.

6. Summary and conclusions

A powerful and flexible full dynamic model of a simple hybrid system has been developed that allows the characterisation of part-load performance and testing of control strategies. From the system configuration and part-load performance, the following control-relevant aspects have been detected:

- The degrees of freedom for the system are fuel flow and air flow. Furthermore fuel utilisation may be varied within certain limits during transients.
- The part-load behaviour of the system shows the presence of unstable regimes (no steady-state exists) at high fuel flow and low air flow, and regimes with very low SOFC temperatures at high air flow and low fuel flow.
- Operation with constant mean SOFC temperature is possible within a wide load range, but the temperature is very unstable in the low load regime. A feedback control of temperature is therefore required.
- Measurable, respectively, calculable inputs to the control system are power, air flow, fuel utilisation and temperature of the fuel leaving the cell.
- Manipulable variables are cell current, fuel flow and generator power.

Based on these aspects, a multi-loop feedback control scheme has been designed. Power is controlled by manipulating the SOFC current; fuel utilisation is controlled by manipulating the fuel flow; air flow is controlled by manipulating generator power; and the mean cell temperature is inferentially controlled by measuring the fuel cell exhaust fuel temperature and correcting the air flow setpoint. The interaction between the control loops does not lead to instability due to the strongly different controller time scales. The setpoints of the air flow and the measured temperature are calculated on the basis of steady-state characteristics of the hybrid system at constant fuel cell temperature operation.

The response of the system to load changes, load curve following, ambient air condition change and incidents of malfunction and degradation is tested. The system was stable during all the tests. The following conclusions on the system response may be drawn:

- Small load changes in the range of few kilowatts are followed in a time scale of below 1 s.
- Large load changes are followed in a time scale of 10–60 s.
- During normal operation, the mean SOFC temperature is stable within a band of 40–65 K around its design value.
- Ambient air conditions have only a small influence on system characteristics, provided their influence on the behaviour between measured and controlled temperature is accounted for.
- Fuel flow measurement errors or variations in fuel quality are severe, as they falsify the calculated control variable of fuel utilisation, which is an important parameter for the system performance. An overestimation of fuel flow by 5% may lead to a steady-state cell temperature offset of approximately 35 K above the design value.
- The temperature variation increases with increasing fuel cell degradation. It may therefore be advisable to readjust the control system characteristics after a certain system degradation.

The depicted quantitative data are only valid for the studied model. However, the qualitative trends are expected to be similar in a genuine system. Hence, the demonstrated methods can be applied on a real system, given that relevant data of its behaviour are available.

Acknowledgements

We thank the Norwegian Research Council, Shell Technology Norway and Statkraft for their financial support.

References

[1] C. Stiller, B. Thorud, S. Seljebø, Ø. Mathisen, H. Karoliussen, O. Bolland, Finite-volume modeling and hybrid-cycle performance of planar and tubular solid oxide fuel cells, J. Power Sources 141 (2005) 227–240.
[2] D. Rao, G.S. Samuelsen, A thermodynamic analysis of tubular SOFC based hybrid systems, ASME Paper 2001-GT-0522.
[3] S.H. Chan, H.K. Ho, Y. Tian, Modeling for part-load operation of solid oxide fuel cell-gas turbine hybrid power plant, J. Power Sources 114 (2003) 213–227.
[4] J. Pålsson, A. Selimovic, L. Sjunnesson, Combined solid oxide fuel cell and gas turbine systems for efficient power and heat generation, J. Power Sources 86 (2000) 442–448.
[5] S.E. Veyo, W.L. Lundberg, S.D. Vora, K.P. Litzinger, Tubular SOFC hybrid power system status, ASME Paper 2003-GT-38943.
[6] E. Achenbach, Response of a solid oxide fuel cell to load change, J. Power Sources 57 (1995) 105–109.
[7] P. Costamagna, L. Magistri, A.F. Massardo, Design and part-load performance of a hybrid system based on a solid oxide fuel cell reactor and a micro gas turbine, J. Power Sources 96 (2001) 352–368.
[8] S. Campanari, Full load and part load performance prediction for integrated SOFC and microturbine systems, J. Eng. Gas Turb. Power 122 (2000) 239–246.
[9] J. Pålsson, A. Selimovic, Design and off-design predictions of a combined SOFC and gas turbine system, ASME Paper 2001-GT-0379.
[10] S. Kimijima, N. Kasagi, Performance evaluation of gas turbine-fuel cell hybrid micro generation system, ASME Paper 2002-GT-30111.
[11] C. Stiller, B. Thorud, O. Bolland, Safe dynamic operation of a simple SOFC/GT hybrid system, ASME Paper 2005-GT-68481.
[12] Y. Zhu, K. Tomsovic, Development of models for analyzing the load-following performance of microturbines and fuel cells, Electric Power Syst. Res. 62 (2002) 1–11.
[13] F. Jurado, Study of molten carbonate fuel cell—microturbine hybrid power cycles, J. Power Sources 111 (2002) 121–129.
[14] A.D. Rao, G.S. Samuelsen, Analysis strategies for tubular solid oxide fuel cell based hybrid systems, J. Eng. Gas Turb. Power 124 (2002) 503–509.
[15] T.W. Song, J.L. Sohn, J.H. Kim, T.S. Kim, S.T. Ro, K. Suzuki, Parametric studies for a performance analysis of an SOFC/MGT hybrid power system based on a quasi-2D model, ASME Paper 2004-GT-53304.

[16] E. Achenbach, E. Riensche, Methane/steam reforming kinetics for solid oxide fuel cells, J. Power Sources 52 (1994) 283–288.
[17] S.C. Singhal, K. Kendall, High Temperature Solid Oxide Fuel Cells—Fundamentals, Design and Applications, Elsevier Ltd., 2003.
[18] F. Marsano, L. Magistri, A.F. Massardo, Ejector performance on a solid oxide fuel cell anodic recirculation system, J. Power Sources 129 (2004) 216–228.
[19] W.M. Kays, A.L. London, Compact Heat Exchangers, McGraw-Hill, 1984.
[20] J. Kurzke, Compressor and Turbine Maps for Gas Turbine Performance Computer Programs—Component Map Collection, vol. 2, Joachim Kurzke, Dachau, Germany, 2004.
[21] gPROMS (General Process Modelling and Simulation Tool), v.2.3.4, Process Systems Enterprise Ltd., London, http://www.psenterprise.com/.
[22] Y. Yi, T.P. Smith, J. Brouwer, A.D. Rao, G.S. Samuelsen, Simulation of a 220 kW hybrid SOFC gas turbine system and data comparison, Electrochem. Soc. Proc. 7 (2003) 1442–1454.
[23] N.H. Johannesen, Ejector Theory and Experiments, Dissertation, Danish Academy of Technical Sciences, Copenhagen, Denmark, 1951.
[24] M.R. Von Spakovsky, D. Rancruel, D. Nelson, S.K. Mazumder, R. Burra, K. Acharya, C. Haynes, R. Williams, R.S. Gemmen, Investigation of system and component performance and interaction issues for solid oxide fuel cell based auxiliary power units responding to changes in application load, in: IECON Proceedings (Industrial Electronics Conference), vol. 2, 2003, pp. 1574–1579.
[25] B. Thorud, C. Stiller, T. Weydahl, O. Bolland, H. Karoliussen, Part-load and load-change simulation of tubular SOFC systems, in: Sixth European Solid Oxide Fuel Cell Forum, Lucerne, Switzerland, 2004.
[26] A. Nakajo, C. Stiller, G. Härkegård, O. Bolland, Modeling of thermal stresses and probability of survival of tubular solid oxide fuel cells, J. Power Sources, doi:10.1016/j.jpowsour.2005.09.004.
[27] G. Stephanopoulos, Chemical Process Control—An Introduction to Theory and Practice, Prentice-Hall Inc., New Jersey, 1984.